

Lithium-storage Properties of Gallic Acid-Reduced Graphene Oxide and Silicon-Graphene Composites

Binghui Xu¹, Jintao Zhang², Yi Gu¹, Zhi Zhang³, Wael Al Abdulla⁴, Nanjundan Ashok Kumar¹, and X. S. Zhao^{1,2,*}

Chengzhong yu

¹*School of Chemical Engineering, The University of Queensland, St. Lucia, Brisbane, QLD 4072, Australia.*

²*Institute of Materials for Energy and Environment, College of Materials Science and Engineering, Qingdao University, Qingdao, P R China.*

³*Materials Engineering, The University of Queensland, St. Lucia, Brisbane, QLD 4072, Australia.*

⁴*Australian Institute for Bioengineering and Nanotechnology (AIBN), The University of Queensland, St Lucia, Brisbane, QLD 4072, Australia.*

*Correspondence to X.S.Z. E-mail: george.zhao@uq.edu.au

Abstract

Graphene oxide (GO) was de-oxygenated using gallic acid under mild conditions to prepare reduced graphene oxide (RGO). The resultant RGO showed a lithium-ion storage capacity of 1280 mA h g⁻¹ at a current density of 200 mA g⁻¹ after 350 cycles when used as an anode for lithium ion batteries. The RGO was further used to stabilize silicon (Si) nanoparticles to prepare silicon-graphene composite electrode materials. Experimental results showed that a composite electrode prepared with a mass ratio of Si:GO = 1:2 exhibited the best lithium ion storage performance.

Keywords: reduced graphene oxide, silicon nanoparticles, anode, battery, lithium-ion

1. Introduction

Graphite, a conventional anode material for lithium-ion batteries (LIBs) has a theoretical capacity of about 372 mA h g^{-1} , limiting the development of advanced LIBs for emerging technologies, such as smart grids and electric vehicles. Graphene-based materials have been shown to be a potential electrode for electrochemical energy storage [1]. In particular, graphene as an anode for LIBs can store more lithium ions than graphite because lithium ions can not only be stored on both sides of graphene sheets, but also on the edges and the covalent sites [2].

The chemical method for producing graphene oxide (GO) from graphite is a feasible approach to mass-produce reduced graphene oxide (RGO). The most commonly used reductants are sodium borohydride and hydrazine [3-5]. Both chemicals are toxic and difficult to handle. Zhao and co-workers [6] have demonstrated that urea is an effective reducing agent in removing oxygen-containing groups from GO for restoring the conjugated electronic structure of graphene. Other eco-friendly reducing agents, such as L-ascorbic acid and green tea polyphenols, have also proved to be able to reduce GO [7-9]. Gallic acid (GA), a natural organic acid with three adjacent hydroxyl groups located at its only benzene ring, has recently been shown to possess a considerable ability to reduce GO [10]. It has been observed that phenolic compounds including GA can function as a stabilizer to prevent RGO sheets from aggregation [10-12]. In the present study, the electrochemical properties of GO samples reduced by GA were investigated and compared with previously reported RGO-based anode materials for LIBs. In addition, the GA-reduced GO was also used to stabilize silicon nanoparticles (SiNPs) to prepare Si@RGO composite materials with different Si/GO mass ratios and their lithium ion storage behaviour was evaluated.

2. Experimental Section

2.1 Material Synthesis

Preparation of RGO. GO was synthesized from natural graphite flake (Sigma Aldrich, 325 mesh) using a modified Hummers method [13]. Deoxygenation was carried out using the following protocol. Briefly, 13 mg GA was dissolved in 20 mL of a GO suspension (2 mg mL^{-1}) under sonication. The suspension was transferred into a 20 mL capped vial and placed into an oil bath at $95 \text{ }^\circ\text{C}$ and stirred for 12 h. The resulting black solids were collected after decanting the upper liquid phase. The collected granules were then soaked in de-ionised water for a week and lyophilized. After subsequent heat treatment in a quartz tube at $700 \text{ }^\circ\text{C}$ for 2 h under a H_2/Ar (5/95, v/v) at a heating rate of $5 \text{ }^\circ\text{C min}^{-1}$, a RGO sample was obtained.

Preparation of Si@RGO composites. The as-prepared RGO was further utilized to stabilize SiNPs as follows. SiNPs were first modified by using poly(diallyldimethylammonium chloride) (PDDA). Briefly, 120 mg of SiNPs (Nanostructured & Amorphous Materials Inc., 40-100 nm) were added to 120 mL de-ionised water, followed by adding 3 g of a 20 wt% PDDA (Sigma Aldrich, MW = 10000-20000) solution under sonication in a water bath (KQ3200DE, 40 kHz). Excess PDDA was washed away using copious amounts of de-ionised water. 20, 40 and 80 mg of the PDDA-modified SiNPs were individually added to 20 mL of the GO suspension ($2 \text{ mg}\cdot\text{mL}^{-1}$) and sonicated for an hour. Later, GA (13 mg) was added to the above mixture and stirred at $95 \text{ }^\circ\text{C}$ in an oil bath 12 h. Homogeneous yellow suspension turned black. Upon sedimentation for a short while, black solids and colourless transparent liquid phase were observed indicating the formation of Si@RGO composite.

2.2. Materials Characterization

Field-emission transmission electron microscope (FETEM) images were collected on a Philips Tecnai F30 operated at 200 kV. Field-emission scanning electron microscope (FESEM) images were obtained from a JEOL 7001 operated at 5.0 kV. X-ray diffraction (XRD) patterns were collected on a German Bruker D8 Advanced X-Ray Diffractometer with Ni filtered Cu K α radiation (40 kV, 30 mA). X-ray photoelectron spectra (XPS) were collected on a Kratos Axis ULTRA X-ray photoelectron spectrometer using a monochromatic Al K α (1486.6 eV) X-ray source and a 165 mm hemispherical electron energy analyzer. Raman spectra were collected on a Thermo-Fischer Almega dispersive Raman instrument. The instrument was fitted with both 633 and 785 nm lasers.

2.3. Electrode preparation and electrochemical measurements

A slurry containing the active material (RGO or Si@RGO) with conductive carbon black (super-P) and polyvinylidene fluoride (PVDF) dissolved in N-methyl-2-pyrrolidone (NMP) in mass ratio of 80:10:10 was prepared and homogenised. The slurry was then coated onto a Cu current collector, assembled into a CR2032 coin-type cells in an argon-filled glove box. Pure lithium metal foil was used as both counter and reference electrode. The electrolyte was 1 M LiPF $_6$ in ethylene carbonate/dimethyl carbonate (1:1, v/v). A Celgard 2400 microporous polypropylene membrane was used as the separator. Cyclic voltammetry (CV) measurements were carried out on a CHI 660D electrochemical workstation at a scan rate of 0.1 mV s $^{-1}$. The discharge and charge measurements of the batteries were performed on a Neware system in the fixed voltage window between 0.005 and 3.500 V for RGO anode, between 0.02 and 1.20 V for Si@RGO composites at room temperature.

3. Results and Discussion

Figures 1A and 1B show the FESEM images of a RGO sample at different magnifications. Crumpled graphene sheets with little aggregation of the sheets is seen, which could be attributed to the stabilisation effect of GA. The Brunauer-Emmett-Teller (BET) surface area and pore volume of RGO were measured to be $120 \text{ m}^2 \text{ g}^{-1}$ and $0.50 \text{ cm}^3 \text{ g}^{-1}$ respectively. Figure 1C shows the XPS spectra of both GO and RGO samples. A drastic decrease in the oxygen content after reduction can be seen. It was estimated that the atom percentage of oxygen in the RGO sample was about 2.0%, significantly less than that in the GO sample (31.1%). The high-resolution C1s XPS spectra of GO and RGO are shown in Figure 1D. The C1s spectrum of GO was deconvoluted with five peak components with binding energies of 284.6, 285.1, 286.9, 287.7 and 288.9 eV, corresponding to C=C (sp^2), C-C (sp^3), C-O (hydroxyl and epoxy), C=O (carbonyl), O-C=O (carboxyl), respectively [10, 11, 14]. Meanwhile, for the RGO sample, no obvious peaks belonging to oxygen containing groups were observed, suggesting a fairly complete reduction of GO. Only one prominent C1s peak was observed at 284.8 eV suggesting the sp^2 graphitic nature of the sample.

Figure 1E shows the XRD patterns of samples. For the GO sample, a wide diffraction peak centered at 9.8° corresponding to an interlayer spacing of 0.901 nm can be seen. The graphite sample displayed a sharp peak at 26.5° (corresponding to an interlayer spacing of 0.335 nm). The XRD results indicated the presence of functional groups and the disordered layers after oxidization and exfoliation. After reduction, a new broad peak appeared at around 26.1° for RGO, corresponding to an interlayer spacing of 0.340 nm fairly close to that of graphite. The new broad peak suggests the removal of oxygen containing functionalities and the partially restoration of the conjugate sp^2 networks in the porous RGO network during the reduction of GO [12, 15].

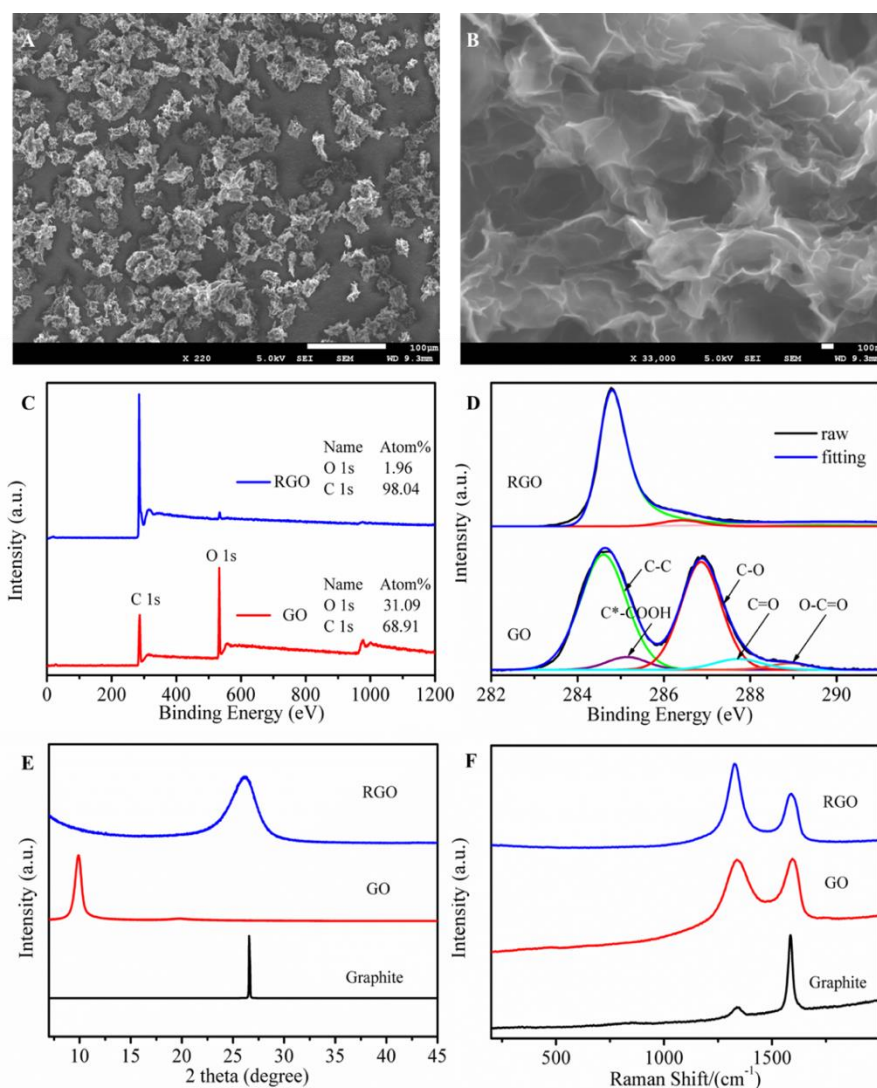


Figure 1. (A-B) FESEM images of RGO under different magnifications; (C) Survey XPS patterns of GO and RGO; (D) C1s XPS patterns of RGO and GO; (E) XRD patterns of RGO, GO and graphite; (F) Raman spectra of RGO, GO, and graphite.

Figure 1F shows the Raman spectra of samples. The pristine graphite displayed a prominent G peak (corresponding to sp^2 hybridizing carbon) at 1581 cm^{-1} , as well as a very small D peak (originating from disordered carbon) at 1338 cm^{-1} . The G band of sample GO was broadened and shifted to 1598 cm^{-1} . The D band at 1342 cm^{-1} became more prominent, indicating the reduction in size of the in-plane sp^2 domains with more defects resulting from the extensive oxidation, thus generating a large number of oxygen-containing groups. While

the Raman spectrum of the RGO sample also contained both G and D bands, the peak intensity ratio of the D band over the G band ($I_D/I_G=1.12$) is higher than that of GO ($I_D/I_G=0.993$). This change in intensity ratio is due to the decrease in the dimension of sp^2 domains during reduction and increased graphitization [14, 16].

Lithium ion storage properties of RGO. The electrochemical performance of the RGO sample was evaluated using CV and charge/discharge techniques. For comparison, graphite was also tested. The specific capacities of the two samples were calculated based on the mass of RGO and graphite, respectively. Figure 2A shows the first three CV curves of the RGO electrode at room temperature. The CV curve of the first cycle was different from those of the subsequent cycles, especially for the cathodic curve. A strong peak at 0.7 V resulted from the irreversible side reactions on the electrode surface due to the solid electrolyte interphase (SEI) film formation. From the second cycle onwards, the CV curves almost overlapped, indicating good reversibility of the RGO electrode.

The discharge-charge profiles of the RGO electrode in the first 3 cycles are shown in Figure 2B. The RGO anode delivered a specific capacity of 1762 mA h g^{-1} in the initial discharging and a reversible capacity of 844 mA h g^{-1} in the first charging. The irreversible capacity can be associated with the formation of the SEI layer in the first cycle. From the second cycle, the curves of RGO anode showed no distinguishable plateaus, which can be attributed to the disordered RGO architecture [17]. It has been proposed that lithium ions can be adsorbed on both sides of a graphene sheet arranged like a ‘house of cards’, leading to two layers of lithium ions on graphene sheet, with a theoretical capacity of 744 mA h g^{-1} through the formation of Li_2C_6 . On the other hand, nano-cavities between RGO sheets due to scrolling and crumpled nature could also contribute to the lithium storage [2].

The cycling performance of the RGO and graphite electrodes was examined at a current density of 200 mA g^{-1} . As is seen from Figure 2C, the RGO electrode delivered a reversible initial discharging capacity of 844 mA h g^{-1} and its reversible capacity maintained a stable rising trend from the 15th cycle. After 200 cycles, the reversible capacity showed a rising trend overall but became more fluctuant. At the 350th cycle, the RGO electrode delivered a reversible capacity of 1280 mA h g^{-1} , which is superior to that of graphite. The possible reason for the fluctuant rising trend of its reversible capacity could be due to slow activation of lithium insertion active sites (e.g., nano-cavities between RGO sheets and edge-type sites) and surface wetting behaviour of the surface by the electrolyte during charging and discharging processes. The stable SEI layer formed during the first cycle can also prohibit further side reactions.

The rate capability of the RGO electrode at current densities ranging from 100 to 2000 mA g^{-1} was studied. As shown in Figure 2D the electrode delivered reversible capacities of about 900, 950, 500, 450, 400 mA h g^{-1} at the current densities of 100, 200, 500, 1000 and 1500 mA g^{-1} , respectively. At 2000 mA g^{-1} , the electrode delivered a capacity of over 350 mA h g^{-1} . After cycling at higher current densities, the electrode delivered even higher reversible capacities when the current densities were lowered. It is believed that edge sites on the RGO (as evidenced from the Raman spectrum in Figure 1F) are beneficial to the improved capacity at high current rates and the porous structure is able to reduce diffusion length of lithium ions, resulting in better rate capability and cycling performance. In addition, the strongly crumpled and scrolled nature of the RGO sheets could also contribute to the structural buffering for the volume expansion during the Li insertion/extraction.

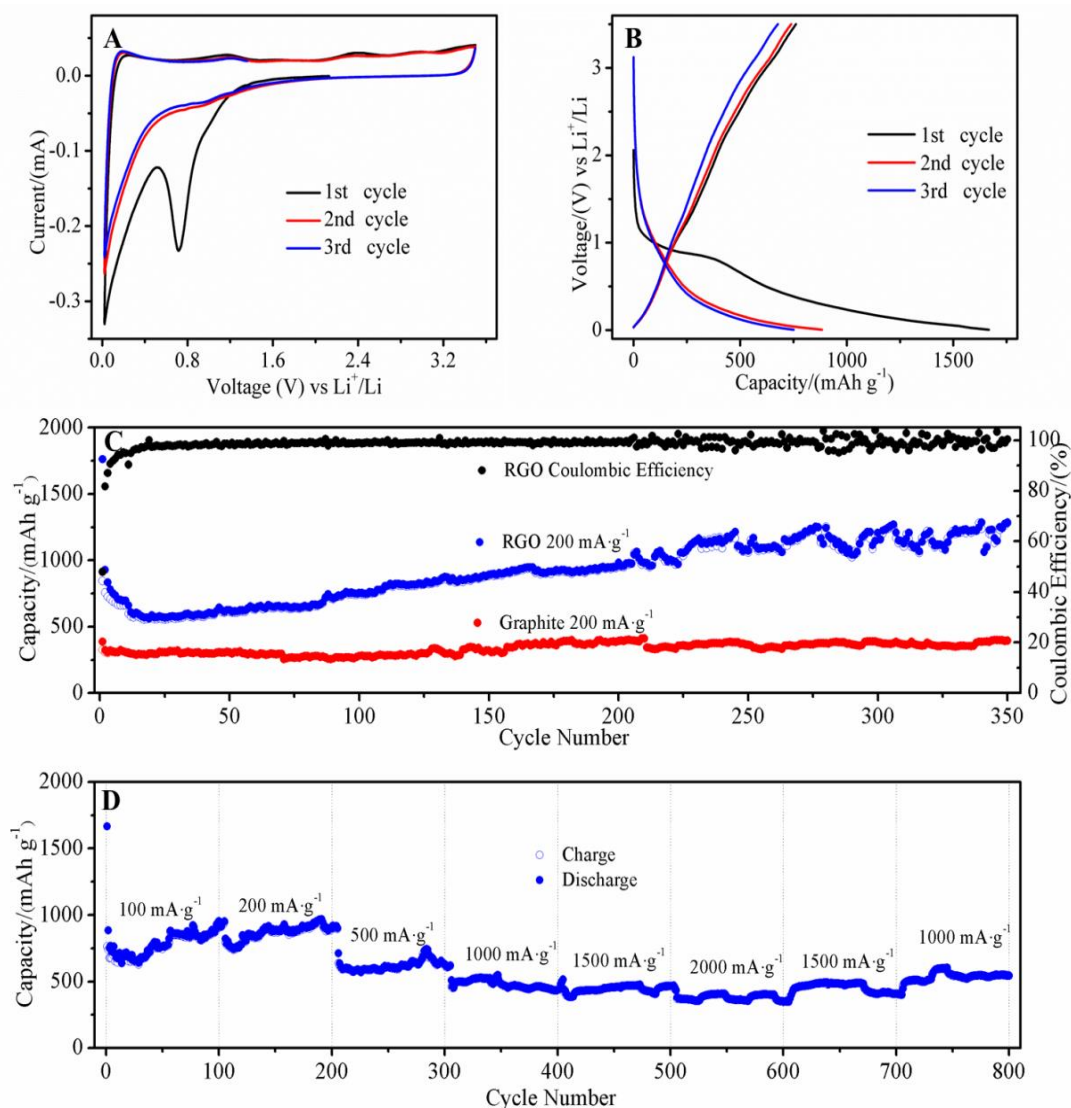


Figure 2. (A) Cyclic voltammetry curves for RGO; (B) galvanostatic discharge-charge profiles of the first three cycles for RGO; (C) cycling performances of RGO and graphite at the current rate of 200 mA·g⁻¹; (D) rate capability of RGO particles.

Table 1 compares the electrochemical performance of RGO materials prepared by using different reducing methods. It can be seen that micron-sized RGO reduced by GA delivered not only high reversible capacity but also exhibited long cycle life. It is worth pointing out that the RGO prepared using GA as a reductant is among the few ecofriendly chemical reducing methods to prepare RGO anode for lithium ion storage without doping or adding extra additives.

Table 1. Electrochemical properties of RGO prepared with different reduction methods

Reducing method	Reversible capacity (mAh·g ⁻¹)	Cycle life	Capacity retention (%)	Current rate (mA·g ⁻¹)
Thermal reduction ^[18]	800	100	81.6	200
Thermal reduction ^[19]	1053	130	–	186
Thermal reduction ^[20]	760	35	–	100
Thermal reduction ^[21]	~634	300	–	1000
Thermal reduction ^[22]	576	50	–	50
Carbothermal reduction ^[23]	~576	20	–	100
Microwave reduction ^[24]	~733	100	–	100
Microwave reduction ^[25]	1002	50	93	40
Photothermal reduction ^[26]	755	50	~60	100
Supercritical reduction ^[27]	1331	100	–	50
Supercritical reduction ^[28]	652	40	–	50
Ascorbic reduction ^[15]	420	100	97	2000
EDA reduction ^[29]	346	60	–	350
Hydrazine reduction ^[30]	~600	50	~48	149
Hydrazine reduction ^[31]	460	100	71	–
GA reduction (this work)	1280	350	–	200

Lithium ion storage properties of Si@RGO composite anode. Silicon (Si) is a promising anode material because of its large theoretical capacity for Li ion storage (Li₂₂Si₅: 4200 mA h g⁻¹; Li₁₅Si₄: 3579 mA h g⁻¹) [32]. However, the severe volume change of bulk Si leads to rapid capacity fading due to pulverization during repetitive lithiation and delithiation processes. In addition, the rate capability of Si is limited by its poor intrinsic electric

conductivity [33, 34]. Two strategies are usually adopted for improving its electrochemical performance. One is to shorten the electronic and ionic transport length by using nano-sized Si particles. However, SiNPs trend to aggregate. The other strategy is to increase the electric conductivity by using carbon materials, such as carbon nanotubes and graphene [2, 35]. Previous studies have shown that graphene can indeed improve the electrochemical performance of SiNPs [36-39].

The FESEM images of a Si@RGO sample prepared using a mass ratio of Si/GO = 1:1 are shown in Figures 3A and 3B. It is seen that SiNPs are well dispersed on the RGO sheets without obvious aggregation. The crumpled RGO layers with a rough texture on the surface were associated with the flexible and corrugated nature. Figures 3B and 3C clearly show that SiNP clusters were wrapped or encapsulated by the continuous corrugated RGO network. The thickness of the Si@RGO particles was about 1 μm (Figure 3C). Such a thin particle morphology is favourable for electrolyte ions to go through, thus enhancing rate capacity. SiNPs wrapped by thin RGO sheets were also seen from the high-resolution TEM image (Figure 3D). The similar size of Si nanoparticles (~ 100 nm) before and after wrapping by RGO sheets indicated that the Si particles did not aggregate during the sample preparation process. The BET surface area and pore volume of Si@RGO were measured to be $95 \text{ m}^2 \text{ g}^{-1}$ and $0.59 \text{ cm}^3 \text{ g}^{-1}$ respectively. The formation of porous RGO network is of importance for the electron transport and is also ideal for accommodating the volume change of the SiNPs during electrochemical reactions. Figures 3E and 3F show the XRD patterns and Raman spectra of Si@RGO, SiNPs and RGO, respectively. All the major XRD and Raman peaks of Si@RGO are overlapped with those of the pristine SiNPs and RGO, indicating that the silicon crystalline structure in the Si@RGO composite are still retained after the freeze-drying and thermal reduction treatment.

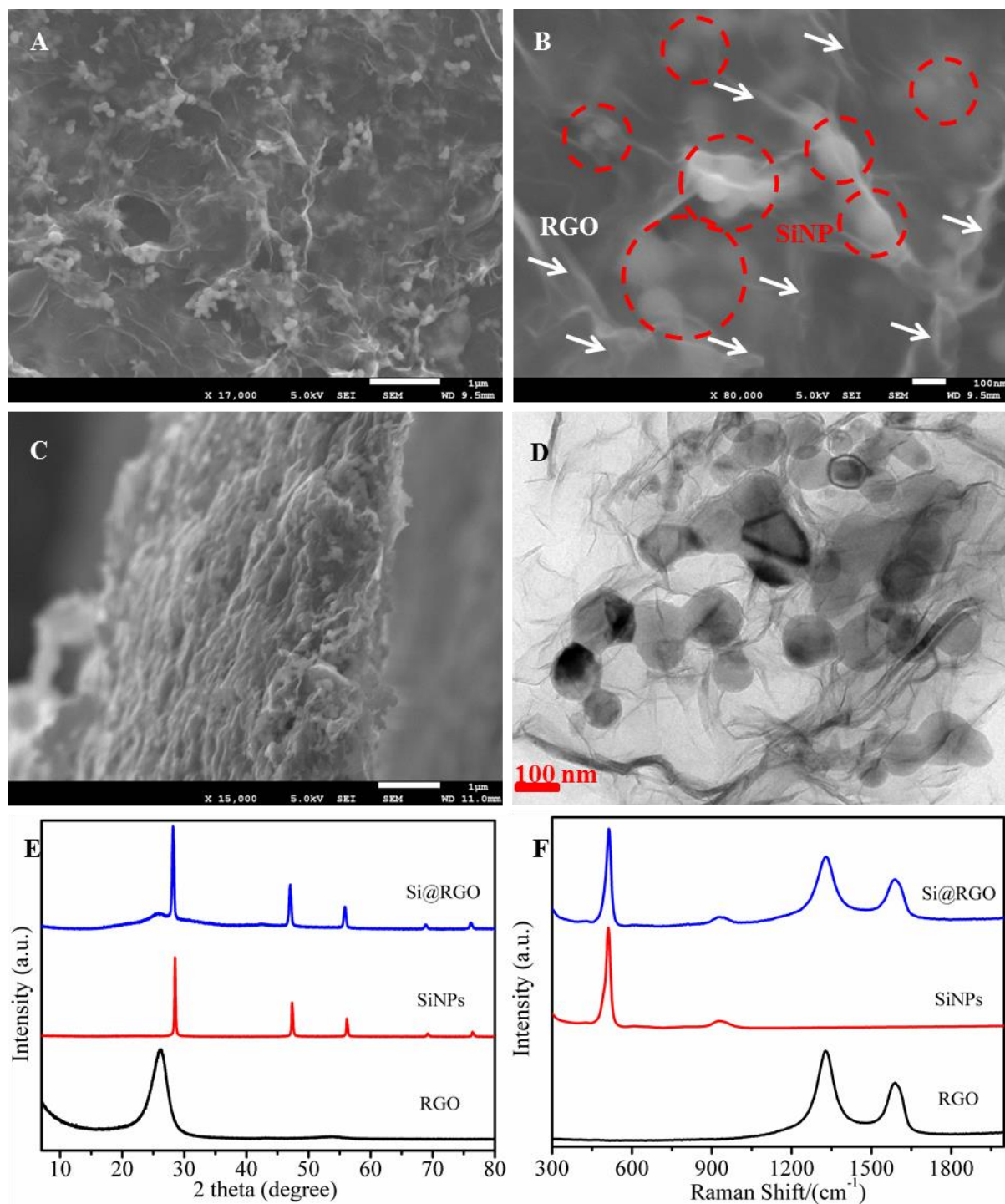


Figure 3. (A and B) Top-view FESEM images of Si@RGO under different magnifications (The white arrows and red circles in Figure 2B show RGO wrapping layers and encapsulated SiNPs, respectively.); (C) cross-sectional view FESEM image of Si@RGO; (D) TEM image of Si@RGO composite; (E) XRD patterns of Si@RGO, SiNPs and RGO; (F) Raman spectra of Si@RGO, SiNPs and RGO.

The electrochemical performance of the Si@RGO composites was studied using CV and charge/discharge techniques. Three samples prepared with Si/GO mass ratios of 1:2, 1:1 and 2:1, respectively, were tested and the results shown in Figure 4. The specific capacity was calculated based on the total mass of Si@RGO. CV curves of Si@RGO 1:2 in the potential range of 0.02 – 1.20 V (versus Li⁺/Li) at a scan rate of 0.1 mV s⁻¹ is shown in Figure 4A. Similar to RGO anode, in the first cycle, a broad cathodic peak due to the formation of SEI was observed at 0.69 V. The absence of the cathodic peak in the subsequent cycles indicated a complete formation of a stable SEI layer in the first cycle. The anodic part showed two peaks at 0.34 and 0.52 V, corresponding to the phase transition of Li–Si alloys to amorphous Si, congruent with previous works [40, 41]. Figure 4B displays the discharge–charge profiles of the Si@RGO 1:2 composite at a current density of 200 mA g⁻¹ in the voltage window of 0.02 to 1.20 V vs. Li⁺/Li. The onset slope at about 0.7 V in the initial discharging curve, which disappeared in the following cycles, corresponded to the SEI formation. Besides, the main discharge plateau was around 0.2 V and charging plateau was around 0.5 V. All these features were in good agreement with the CV curve. The initial discharge/charge capacities were 898 and 1608 mA h g⁻¹, respectively. As a result, the initial Coulombic efficiency was about 55.8 %. The observed initial irreversible capacity of the Si@RGO anode was attributed to the SEI formation and the existence of silicon dioxide on the surface of the SiNPs, both of which consumed Li⁺ ions [42, 43]. From the second cycle, the Coulombic efficiency gradually increased and stabilized. The cycling performance of samples Si@RGO 1:2, 1:1 and 2:1 at a current density 200 mA g⁻¹ for 100 cycles are shown in Figure 4C. Overall, the reversible capacities of all the three samples followed a descending trend. Si@RGO with mass ratio 1:2 delivered the most stable capacity throughout the 100 cycles, (1074 mA h g⁻¹ at the 5th cycle and 900 mA h g⁻¹ at the 100th cycle) with a capacity retention of about 84%. For sample Si@RGO 1:1, the highest reversible capacity was 1270

mA h g^{-1} observed at the 5th cycle. At the 40th cycle, it could still deliver a reversible capacity of 1094 mA h g^{-1} with a capacity retention of about 86 %. After that, fast capacity fading was observed and the reversible capacity could only maintain 526 mA h g^{-1} at the 100th cycle with a capacity retention of about 41 %. For sample Si@RGO 2:1, the highest reversible capacity was 1700 mA h g^{-1} observed at the 5th cycle. At the 30th cycle, it delivered a reversible capacity of 1477 mA h g^{-1} with a capacity retention of about 87 %. More severe capacity fading was observed since then and the battery could only maintain a reversible capacity of 466 mA h g^{-1} at the 100th cycle with a capacity retention of about 27 %.

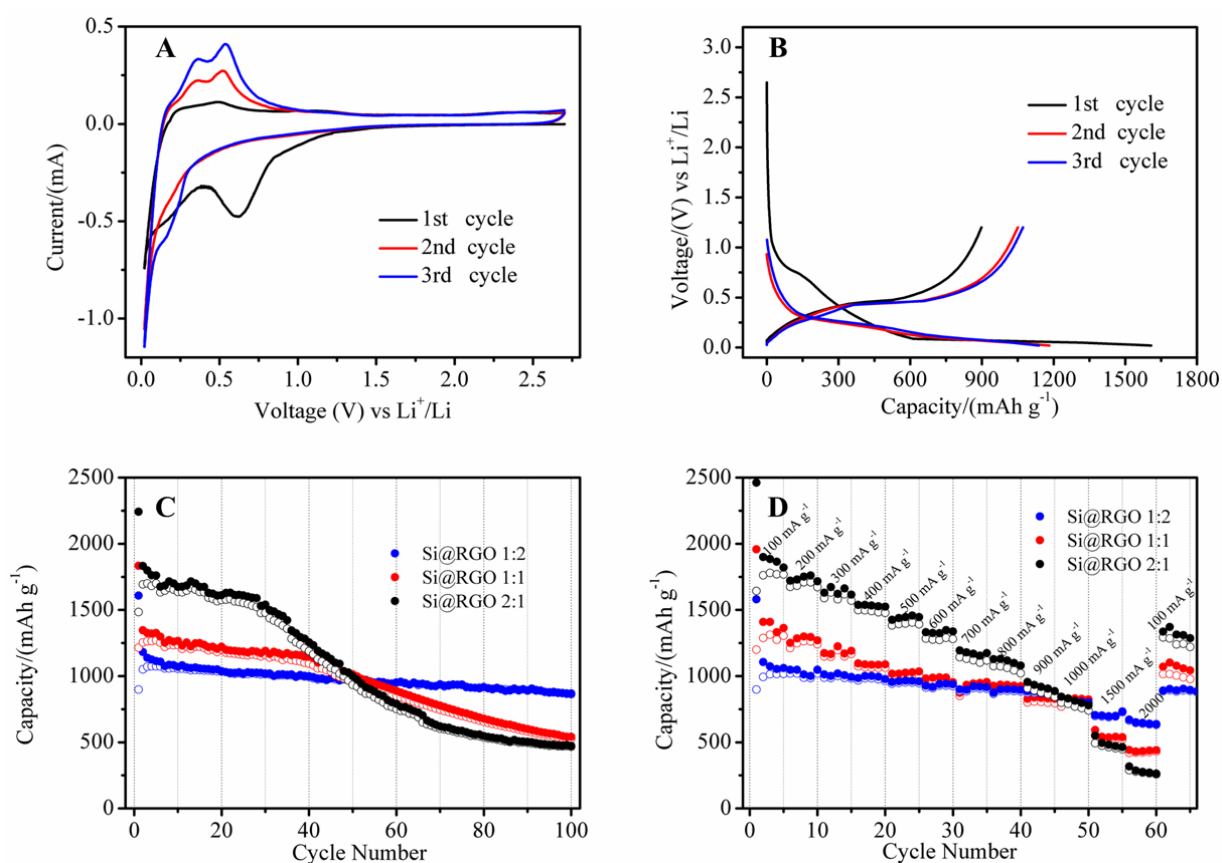


Figure 4. (A) Cyclic voltammetry curves for Si@RGO 1:2 composite; (B) Galvanostatic discharge-charge profiles of the first three cycles; (C) cycling performances of Si@RGO composites with different Si/RGO mass ratios at a current density 200 mA g^{-1} ; (D) rate capabilities of Si@RGO composites with different Si/RGO mass ratios.

The rate capabilities of samples Si@RGO 1:2, Si@RGO 1:1 and Si@RGO 2:1 with current densities ranging from 100 to 2000 mA g⁻¹ are shown in Figure 4D. The Si@RGO 1:2 battery delivered a reversible capacity of about 800 and 650 mA h g⁻¹, when the current density was increased to 1000 and 2000 mA g⁻¹, respectively. On the contrary, although higher starting reversible capacities were seen for samples Si@RGO 1:1 and 2:1 batteries, they delivered only about 520 and 420, 450 and 270 mA h g⁻¹, respectively when the current density was increased to 1000 and 2000 mA g⁻¹. Particularly, when the current density was lowered to 100 mA g⁻¹ after cycling at higher densities, for sample Si@RGO 1:2 the reversible capacity was about 900 mA h g⁻¹. In comparison with the highest capacity of 1019 mA h g⁻¹ at the 6th cycle, this electrode had a capacity retention of 88 %, indicating a good stability of the electrode in a wide range of discharge/charge currents. For samples Si@RGO 1:1 and Si@RGO 2:1, the values were 1000/1313, 76 % and 1250/1779, 70 %, respectively. It can be concluded that among the three prepared Si@RGO composites, sample Si@RGO 1:2 delivered both the most stable cycling performance and the best rate capability. Table 2 compares the capacity and cycling stability of electrode Si@RGO 1:2 with that of those Si-graphene composite electrode materials reported in the literature.

Table 2. Comparison of electrochemical properties of Si@RGO 1:2 with that of some Si-graphene composite electrode materials reported in the literature

Material/Remark	Reversible capacity (mAh·g ⁻¹)	Cycle life	Capacity retention (%)	Current rate (mA·g ⁻¹)	Reference
Silicon-Reduced Graphene Oxide/ electroless etching and graphene self-encapsulating	>1000	50	–	1000	[44]
Si-Graphene Nanocomposites/ magnesiothermic reduction, freeze-drying, and thermal reduction	746	160	–	1000	[45]
Si embedded porous carbon graphene hybrid film/ alternatively stacked Si-porous carbon layers and graphene layers	765	100	75	200	[46]
Si porous rGO composite/ steam etching of Si rGO aerogel	1004	100	–	50	[47]
Si graphene nanocomposite/ low-molecular weight polyacrylic acid -functionalized graphene oxide	1000	100	80	500	[48]
Graphene-encapsulated SiNP Aerogel/ freeze-drying	617	50	–	800	[49]
This work	900	100	84	200	

Conclusions

In summary, RGO sheets prepared by reducing GO with gallic acid displayed a good electrochemical performance when used as anode for LIBs with a reversible capacity of around 1280 mA h g⁻¹ after 350 cycles at a current density of 200 mA g⁻¹ as well as a good rate capability. The gallic-acid-reduced GO sheets were found to be a good support for Si nanoparticles. A composite containing RGO and Si nanoparticles exhibited a capacity of 900 mA h g⁻¹ at the 100th cycle, a capacity retention of 84% with excellent rate capability. A good coverage of Si nanoparticles by RGO sheets can not only buffer the volume changes of the Si

nanoparticles during charge/discharge to prevent the particle from aggregation, but also improve the overall ionic and electrical conductivities of the composite electrode.

Acknowledgements

The University of Queensland is acknowledged for supporting this research work under the Vice-Chancellor's Research and Teaching Fellowship Program (Ref: 2015000144). The facilities and technical assistance of the Australian Microscopy and Microanalysis Research Facility at the Centre for Microscopy and Microanalysis at the University of Queensland are acknowledged. B. H. X thanks the China Scholarship Council for support.

References

- [1] E.J. Yoo, J. Kim, E. Hosono, H. Zhou, T. Kudo, I. Honma, Large reversible Li storage of graphene nanosheet families for use in rechargeable lithium ion batteries, *Nano Lett.*, 8 (2008) 2277-2282.
- [2] C. Xu, B. Xu, Y. Gu, Z. Xiong, J. Sun, X. Zhao, Graphene-based electrodes for electrochemical energy storage, *Energy Environ. Sci.*, 6 (2013) 1388-1414.
- [3] H.J. Shin, K.K. Kim, A. Benayad, S.M. Yoon, H.K. Park, I.S. Jung, M.H. Jin, H.K. Jeong, J.M. Kim, J.Y. Choi, Efficient reduction of graphite oxide by sodium borohydride and its effect on electrical conductance, *Adv. Funct. Mater.*, 19 (2009) 1987-1992.
- [4] S. Stankovich, R.D. Piner, X. Chen, N. Wu, S.T. Nguyen, R.S. Ruoff, Stable aqueous dispersions of graphitic nanoplatelets via the reduction of exfoliated graphite oxide in the presence of poly (sodium 4-styrenesulfonate), *J. Mater. Chem.*, 16 (2006) 155-158.

- [5] Y. Liu, R. Wang, X. Yan, Synergistic Effect between Ultra-Small Nickel Hydroxide Nanoparticles and Reduced Graphene Oxide sheets for the Application in High-Performance Asymmetric Supercapacitor, *Scientific reports*, 5 (2015).
- [6] Z.B. Lei, L. Lu, X.S. Zhao, The electrocapacitive properties of graphene oxide reduced by urea, *Energy Environ. Sci.*, 5 (2012) 6391-6399.
- [7] J. Zhang, H. Yang, G. Shen, P. Cheng, J. Zhang, S. Guo, Reduction of graphene oxide vial-ascorbic acid, *Chem. Commun.*, 46 (2010) 1112-1114.
- [8] Y. Wang, Z. Shi, J. Yin, Facile synthesis of soluble graphene via a green reduction of graphene oxide in tea solution and its biocomposites, *ACS Appl. Mater. Int.*, 3 (2011) 1127-1133.
- [9] O. Akhavan, M. Kalaei, Z. Alavi, S. Ghiasi, A. Esfandiari, Increasing the antioxidant activity of green tea polyphenols in the presence of iron for the reduction of graphene oxide, *Carbon*, 50 (2012) 3015-3025.
- [10] J. Li, G. Xiao, C. Chen, R. Li, D. Yan, Superior dispersions of reduced graphene oxide synthesized by using gallic acid as a reductant and stabilizer, *J. Mater. Chem. A*, 1 (2013) 1481-1487.
- [11] J. Wang, Z. Shi, J. Fan, Y. Ge, J. Yin, G. Hu, Self-assembly of graphene into three-dimensional structures promoted by natural phenolic acids, *J. Mater. Chem.*, 22 (2012) 22459-22466.
- [12] Y. Lei, Z. Tang, R. Liao, B. Guo, Hydrolysable tannin as environmentally friendly reducer and stabilizer for graphene oxide, *Green Chem.*, 13 (2011) 1655-1658.

- [13] Z.G. Xiong, L.L. Zhang, J.Z. Ma, X.S. Zhao, Photocatalytic degradation of dyes over graphene-gold nanocomposites under visible light irradiation, *Chem. Commun.*, 46 (2010) 6099-6101.
- [14] S. Stankovich, D.A. Dikin, R.D. Piner, K.A. Kohlhaas, A. Kleinhammes, Y. Jia, Y. Wu, S.T. Nguyen, R.S. Ruoff, Synthesis of graphene-based nanosheets via chemical reduction of exfoliated graphite oxide, *Carbon*, 45 (2007) 1558-1565.
- [15] K. Shu, C. Wang, S. Li, C. Zhao, Y. Yang, H. Liu, G. Wallace, Flexible free-standing graphene paper with interconnected porous structure for energy storage, *J. Mater. Chem. A*, 3 (2015) 4428-4434.
- [16] N.A. Kumar, M. Togami, Y. Oishi, M. Tominaga, M. Takafuji, H. Ihara, Iron metal induced deoxygenation of graphite oxide nanosheets-insights on the capacitive properties of binder-free electrodes, *RSC Adv.*, 5 (2015) 23367-23373.
- [17] P. Guo, H. Song, X. Chen, Electrochemical performance of graphene nanosheets as anode material for lithium-ion batteries, *Electrochem. Commun.*, 11 (2009) 1320-1324.
- [18] J. Zhang, B. Guo, Y. Yang, W. Shen, Y. Wang, X. Zhou, H. Wu, S. Guo, Large scale production of nanoporous graphene sheets and their application in lithium ion battery, *Carbon*, 84 (2015) 469-478.
- [19] Y. Jiang, Z.-J. Jiang, S. Cheng, M. Liu, Fabrication of 3-Dimensional Porous Graphene Materials for Lithium Ion Batteries, *Electrochimica Acta*, 146 (2014) 437-446.
- [20] D. Cai, L. Ding, S. Wang, Z. Li, M. Zhu, H. Wang, Facile synthesis of ultrathin-shell graphene hollow spheres for high-performance lithium-ion batteries, *Electrochimica Acta*, 139 (2014) 96-103.

- [21] D. Cai, S. Wang, L. Ding, P. Lian, S. Zhang, F. Peng, H. Wang, Superior cycle stability of graphene nanosheets prepared by freeze-drying process as anodes for lithium-ion batteries, *J. Power Sources*, 254 (2014) 198-203.
- [22] X. Liu, H. Zhao, X. Huang, Y. Hu, H. Gao, X. Liu, L. Shen, Fabrication of flexible graphene paper and its electrochemical properties used in lithium ion batteries, *The European Physical Journal Applied Physics*, 66 (2014) 30301.
- [23] R. Mei, X. Song, Y. Hu, Y. Yang, J. Zhang, Hollow reduced graphene oxide microspheres as a high-performance anode material for Li-ion batteries, *Electrochimica Acta*, 153 (2015) 540-545.
- [24] L.-l. Liu, M.-z. An, P.-x. Yang, J.-q. Zhang, Few-layer Graphene Prepared Via Microwave Digestion Reduction and its Electrochemical Performances in Lithium Ion Batteries, *Int. J. Electrochem. Sci*, 10 (2015) 1582-1594.
- [25] W. Ahn, H.S. Song, S.-H. Park, K.-B. Kim, K.-H. Shin, S.N. Lim, S.-H. Yeon, Morphology-controlled graphene nanosheets as anode material for lithium-ion batteries, *Electrochimica Acta*, 132 (2014) 172-179.
- [26] H. Guo, M. Peng, Z. Zhu, L. Sun, Preparation of reduced graphene oxide by infrared irradiation induced photothermal reduction, *Nanoscale*, 5 (2013) 9040-9048.
- [27] D. Yoon, K.Y. Chung, W. Chang, S.M. Kim, M.J. Lee, Z. Lee, J. Kim, Hydrogen-Enriched Reduced Graphene Oxide with Enhanced Electrochemical Performance in Lithium Ion Batteries, *Chem. Mat.*, 27 (2014) 266-275.
- [28] E.B. Nursanto, A. Nugroho, S.-A. Hong, S.J. Kim, K.Y. Chung, J. Kim, Facile synthesis of reduced graphene oxide in supercritical alcohols and its lithium storage capacity, *Green Chem.*, 13 (2011) 2714-2718.

- [29] J. Li, L. Li, B. Zhang, M. Yu, H. Ma, J. Zhang, C. Zhang, J. Li, Synthesis of Few-Layer Reduced Graphene Oxide for Lithium-Ion Battery Electrode Materials, *Ind. Eng. Chem. Res.*, 53 (2014) 13348-13355.
- [30] Ó. Vargas, Á. Caballero, J. Morales, Deficiencies of Chemically Reduced Graphene as Electrode in Full Li-Ion Cells, *Electrochimica Acta*, 165 (2015) 365-371.
- [31] G. Wang, X. Shen, J. Yao, J. Park, Graphene nanosheets for enhanced lithium storage in lithium ion batteries, *Carbon*, 47 (2009) 2049-2053.
- [32] S.B. Son, B. Kappes, C. Ban, Surface Modification of Silicon Anodes for Durable and High-Energy Lithium-Ion Batteries, *Israel Journal of Chemistry*, 55 (2015) 558-569.
- [33] X. Su, Q. Wu, J. Li, X. Xiao, A. Lott, W. Lu, B.W. Sheldon, J. Wu, Silicon-Based Nanomaterials for Lithium-Ion Batteries: A Review, *Adv. Energy Mater.*, 4 (2014) 1-23.
- [34] J.R. Szczech, S. Jin, Nanostructured silicon for high capacity lithium battery anodes, *Energy Environ. Sci.*, 4 (2011) 56-72.
- [35] Z. Xiu, X. Hao, Y. Wu, Q. Lu, S. Liu, Graphene-bonded and-encapsulated mesoporous TiO₂ microspheres as a high-performance anode material for lithium ion batteries, *J. Power Sources*, 287 (2015) 334-340.
- [36] H. Tang, Y. Zhang, Q. Xiong, J. Cheng, Q. Zhang, X. Wang, C. Gu, J. Tu, Self-assembly silicon/porous reduced graphene oxide composite film as a binder-free and flexible anode for lithium-ion batteries, *Electrochimica Acta*, 156 (2015) 86-93.
- [37] B.P.N. Nguyen, N.A. Kumar, J. Gaubicher, F. Duclairoir, T. Brousse, O. Crosnier, L. Dubois, G. Bidan, D. Guyomard, B. Lestriez, Nanosilicon-Based Thick

- Negative Composite Electrodes for Lithium Batteries with Graphene as Conductive Additive, *Adv. Energy Mater.*, 3 (2013) 1351-1357.
- [38] J. Chang, X. Huang, S. Cui, S. Mao, J. Chen, Three-dimensional carbon-coated Si/rGO Nanostructures anchored by nickel foam with carbon Nanotubes for li-ion battery applications, *Nano Energy*, 15 (2015) 679–687.
- [39] T. Mori, C.-J. Chen, T.-F. Hung, S.G. Mohamed, Y.-Q. Lin, H.-Z. Lin, J.C. Sung, S.-F. Hu, R.-S. Liu, High specific capacity retention of graphene/silicon nanosized sandwich structure fabricated by continuous electron beam evaporation as anode for lithium-ion batteries, *Electrochimica Acta*, 165 (2015) 166-172.
- [40] X. Zhou, Y.-X. Yin, A.-M. Cao, L.-J. Wan, Y.-G. Guo, Efficient 3D conducting networks built by graphene sheets and carbon nanoparticles for high-performance silicon anode, *ACS Appl. Mater. Int.*, 4 (2012) 2824-2828.
- [41] Y. Zhu, W. Liu, X. Zhang, J. He, J. Chen, Y. Wang, T. Cao, Directing Silicon–Graphene Self-Assembly as a Core/Shell Anode for High-Performance Lithium-Ion Batteries, *Langmuir*, 29 (2013) 744-749.
- [42] J. Deng, H. Ji, C. Yan, J. Zhang, W. Si, S. Baunack, S. Oswald, Y. Mei, O.G. Schmidt, Naturally Rolled-Up C/Si/C Trilayer Nanomembranes as Stable Anodes for Lithium-Ion Batteries with Remarkable Cycling Performance, *Angew. Chem.*, 125 (2013) 2382-2386.
- [43] H.F. Xiang, K. Zhang, G. Ji, J.Y. Lee, C.J. Zou, X.D. Chen, J.S. Wu, Graphene/nanosized silicon composites for lithium battery anodes with improved cycling stability, *Carbon*, 49 (2011) 1787-1796.
- [44] X. Gao, J. Li, Y. Xie, D. Guan, C. Yuan, A Multilayered Silicon-Reduced Graphene Oxide Electrode for High Performance Lithium-Ion Batteries, *ACS Appl. Mater. Int.*, 7 (2015) 7855-7862.

- [45] D. He, F. Bai, L. Li, L. Shen, H.H. Kung, N. Bao, Fabrication of Sandwich-structured Si Nanoparticles-Graphene Nanocomposites for High-performance Lithium-ion Batteries, *Electrochimica Acta*, 169 (2015) 409-415.
- [46] J. Wu, X. Qin, H. Zhang, Y.-B. He, B. Li, L. Ke, W. Lv, H. Du, Q.-H. Yang, F. Kang, Multilayered silicon embedded porous carbon/graphene hybrid film as a high performance anode, *Carbon*, 84 (2015) 434-443.
- [47] H. Tang, J. Zhang, Y. Zhang, Q. Xiong, Y. Tong, Y. Li, X. Wang, C. Gu, J. Tu, Porous reduced graphene oxide sheet wrapped silicon composite fabricated by steam etching for lithium-ion battery application, *J. Power Sources*, 286 (2015) 431-437.
- [48] F. Maroni, R. Raccichini, A. Birrozzi, G. Carbonari, R. Tossici, F. Croce, R. Marassi, F. Nobili, Graphene/silicon nanocomposite anode with enhanced electrochemical stability for lithium-ion battery applications, *J. Power Sources*, 269 (2014) 873-882.
- [49] X. Hu, Y. Jin, B. Zhu, Y. Tan, S. Zhang, L. Zong, Z. Lu, J. Zhu, Free-Standing Graphene-Encapsulated Silicon Nanoparticle Aerogel as an Anode for Lithium Ion Batteries, *ChemNanoMat*, (2016).